CAMBRIDGE
UNIVERSITY PRESS

RESEARCH PAPER

Discovery of the most luminous quasar of the last 9 Gyr

Christopher A. Onken,[1] Samuel Lai(賴民希),[2] Christian Wolf,[3] Adrian B. Lucy,[4] Wei Jeat Hon,[5] Patrick Tisserand,[6] Jennifer L. Sokoloski,[7] Gerardo J. M. Luna,[8] Rajeev Manick,[9] Xiaohui Fan,[10] and Fuyan Bian (边福彦)[11]

[1] Research School of Astronomy and Astrophysics, Australian National University, Canberra ACT 2611, Australia

[2] Research School of Astronomy and Astrophysics, Australian National University, Canberra ACT 2611, Australia

[3] Research School of Astronomy and Astrophysics, Australian National University, Canberra ACT 2611, Australia;
Centre for Gravitational Astrophysics, Australian National University, Canberra ACT 2600, Australia

[4] Space Telescope Science Institute, 3700 San Martin Drive, Baltimore, MD 21218, USA

[5] School of Physics, University of Melbourne, Parkville, Victoria 3010, Australia

[6] Sorbonne Universités, UPMC Univ Paris 6 et CNRS, Institut d'Astrophysique de Paris, 98 bis bd Arago, F-75014 Paris, France

[7] Columbia Astrophysics Lab 550 W120th Street, 1027 Pupin Hall, MC 5247, Columbia University, New York, NY 10027, USA

[8] CONICET-Universidad de Buenos Aires, Instituto de Astronomía y Física del Espacio (IAFE), Av. Inte. Güiraldes 2620, C1428ZAA, Buenos Aires, Argentina;
Universidad de Buenos Aires, Facultad de Ciencias Exactas y Naturales, Buenos Aires, Argentina;
Universidad Nacional de Hurlingham, Av. Gdor. Vergara 2222, Villa Tesei, Buenos Aires, Argentina

[9] Univ. Grenoble Alpes, CNRS, IPAG, 38000 Grenoble, France;
South African Astronomical Observatory, PO Box 9, Observatory 7935, South Africa

[10] Steward Observatory, University of Arizona, 933 North Cherry Avenue, Tucson, AZ 85721, USA

[11] European Southern Observatory, Alonso de Córdova 3107, Casilla 19001, Vitacura, Santiago 19, Chile

Author for correspondence: Christopher A. Onken, Email: christopher.onken@anu.edu.au.

Abstract

We report the discovery of a bright (g = 14.5 mag (AB), K = 11.9 mag (Vega)) quasar at redshift z = 0.83 – the optically brightest (unbeamed) quasar at $z > 0.4$. SMSS J114447.77-430859.3, at a Galactic latitude of b = +18.1°, was identified by its optical colours from the SkyMapper Southern Survey (SMSS) during a search for symbiotic binary stars. Optical and near-infrared spectroscopy reveals broad Mg II, Hβ, Hα, and Paβ emission lines, from which we measure a black hole mass of $\log_{10}(M_{BH}/M_\odot)$ = 9.4 ± 0.5. With its high luminosity, L_{bol} = (4.7 ± 1.0) × 10^{47} erg s^{-1} or $M_i(z = 2)$ = −29.74 mag (AB), we estimate an Eddington ratio of ≈ 1.4. As the most luminous quasar known over the last ∼9 Gyr of cosmic history, having a luminosity 8× greater than 3C 273, the source offers a range of potential follow-up opportunities.

Keywords: active galactic nuclei: quasars; supermassive black holes

1. INTRODUCTION

The observational study of quasars took off rapidly from the back-to-back-to-back papers of *Nature*'s 16 March 1963 issue, which featured the redshift determinations for 3C 273 and 3C 48 (Schmidt 1963; Oke 1963; Greenstein 1963). Barely two years later, the quasar 3C 9 became the first known object at a redshift greater than 2 (Schmidt 1965). But as exemplified by the 5-magnitude difference in the optical brightness between 3C 273 and 3C 9, the exploration towards higher redshifts became a push to fainter magnitudes.

Fortunately, the early recognition of radio-quiet quasars becoming prominent amongst blue, star-like objects beyond a magnitude of V = 14.5 (Vega) provided an efficient means of identifying quasars from photometric techniques (Sandage 1965) and known quasars now number in the hundreds of thousands (see, e.g., the Million Quasar Catalogue, v7.5, hereafter Milliquas; Flesch 2021). Despite the proliferation of wide-area surveys across a range of wavelengths over the intervening fifty years, the search for bright quasars remains unfinished.

Here, we report on a spectroscopic investigation of a bright, blue, point-like source selected from the SkyMapper Southern Survey Data Release 2 (SMSS DR2; Wolf et al. 2018b; Onken et al. 2019), which demonstrates that SMSS J114447.77-430859.3 (SMSS DR2 object_id[a] 84280208; hereafter, J1144) is a z = 0.83 quasar. Aside from one blazar object at z = 0.6 (PKS 1424+240), this makes J1144 the optically brightest quasar known above a redshift of 0.4.

Spectroscopy of J1144 was first acquired during a search for symbiotic binaries, in which cool giant stars accrete onto smaller companions, using SMSS DR2 (Lucy 2021). While any known active galactic nucleus (AGN, as identified in SIMBAD; Wenger et al. 2000) was excluded, J1144 had only been identified as an AGN *candidate* by its near-IR and IR colours. It was identified as a candidate by Edelson & Malkan (2012) using the Two Micron All-Sky Survey (2MASS; Skrutskie et al. 2006) and the *Wide-field Infrared Survey Explorer* (*WISE*; Wright et al. 2010; Mainzer et al. 2011). Similarly, Secrest

---

[a]The name and object_id remain the same in SMSS DR3.

et al. (2015) utilised the AllWISE[b] update to the IR dataset and selected J1144 as a quasar candidate from its IR colours alone. Notably, Shu et al. (2019) even estimated a photometric redshift for J1144 of $z = 0.82$ from DR2 of the *Gaia* satellite mission (Gaia Collaboration & et al. 2016; Gaia Collaboration 2018) and the unWISE (Schlafly et al. 2019) revision to the photometry from *WISE*.

However, the *WISE* colours of symbiotic stars sometimes fall in typical AGN selection regimes, which is why such sources were not excluded from the symbiotic star search. In fact, the flickering, accretion-powered symbiotic star EF Aql has an AGN-like $(W1 - W2) \approx 0.9$ colour and was discovered via the UV-bright Quasar Survey (UVQS; Monroe et al. 2016; Margon et al. 2016; Zamanov et al. 2017). Lucy (2021) explored various SMSS selection mechanisms for different types of symbiotic stars, and J1144, being much bluer than most isolated cool giant stars, was caught by a $(u-g)/(u-v)$ colour-only selection. Thus, along with 232 other symbiotic star candidates, optical spectroscopy of J1144 was obtained with the goal of confirming the presence of a cool giant star with emission lines, indicative of symbiotic binarity. J1144 was the only observed source to show AGN emission lines.

In § 2, we describe the observations and data processing. In § 3, we analyse the spectroscopic data and estimate the mass of the central black hole (BH). We summarise additional data available for J1144 in § 4 and compare J1144 to other bright quasars in § 5. § 6 discusses the outlook to further study and utilisation of J1144, as well as the prospects for additional such discoveries in the future. Throughout the paper, we use Vega magnitudes for *Gaia* and IR data, and AB magnitudes for the SkyMapper passbands: *uvgriz*. We adopt a flat ΛCDM cosmology with $\Omega_m = 0.3$ and a Hubble-Lemaître constant of $H_0 = 70$ km sec^{-1} Mpc^{-1}.

2. OBSERVATIONS AND DATA PROCESSING

The spectroscopic portion of the symbiotic star program (described in Lucy 2021) principally used the South African Astronomical Observatory (SAAO) 1.9-meter telescope and its SpUpNIC instrument (Spectrograph Upgrade: Newly Improved Cassegrain; Crause et al. 2019). Following the initial classification of J1144 as an AGN, additional optical spectroscopic data was obtained at higher spectral resolution with the Australian National University (ANU) 2.3-meter telescope at Siding Spring Observatory (SSO) using the Wide Field Spectrograph (WiFeS; Dopita et al. 2007, 2010), and near-IR spectroscopy was obtained with the TripleSpec4.1 instrument (Schlawin et al. 2014) on the Southern Astrophysical Research (SOAR) 4.1-meter telescope.

2.1 Optical spectroscopy with SAAO 1.9m / SpUpNIC

SpUpNIC observations of J1144 were obtained on UT 2019-06-24 with the G7 grating. G7 is a low-resolution grating, which covered $3300 - 8930$ Å with a resolving power R∼500. A BG38 filter was manually inserted into the arc beam. The

spectroscopic slit width was 2.24 arcsec in seeing of $\sim 2''$, and a spatial binning of 2 pixels was used. The exposure time was 1200 s, with the object at an airmass of 1.2.

Flux calibration was performed with observations of the spectrophotometric standard star, CD–32 9927 (Hamuy et al. 1994)[c], obtained on the same night. Data reduction, including bias subtraction and flat-fielding, used the standard tasks in the Image Reduction and Analysis Facility (IRAF; Tody 1986). A second pass at flux scaling was performed by processing the spectrophotometric standard in the same way as the science spectra and determining the residual correction needed to align the flux with the model values. The final signal-to-noise ratio (S/N) of the SpUpNIC spectrum was ~ 50 per pixel.

2.2 Optical spectroscopy with ANU 2.3m / WiFeS

WiFeS spectra were obtained on UT 2022-03-11 with two grating configurations. WiFeS is an integral field spectrograph and when used with a spatial binning of 2 pixels, it provides $1x1$ arcsec sampling over its $25x38$ arcsec field-of-view.

With the resolving power R∼3000 gratings, an exposure of 600 s was obtained, covering the wavelength range $3250 - 9550$ Å across the two cameras of the spectrograph (the RT560 beamsplitter was used). For the high-resolution gratings (R∼7000), an exposure time of 900 s was used. The B7000 grating covered $4180 - 5540$ Å, while the I7000 grating covered $6810 - 9040$ Å. All observations were obtained near an airmass of 1.2 with seeing of $1.8 - 2$ arcsec in the *i*-band.

The spectrophotometric standard star, BD–12 2669 (Heap & Lindler 2010), was observed immediately after the J1144 spectra. The raw frames were reduced with the PYTHON-based pipeline, PyWiFeS (Childress et al. 2014). We then extracted the spectra from the calibrated 3D data cubes using QFitsView[d], selecting nearby source-free regions for sky subtraction. Variance and data-quality frames were extracted from the same regions. As with the SAAO data, a second iteration of flux scaling was performed by aligning the processed spectrophotometric standard spectrum to the model fluxes. The S/N in the final spectra ranged from 20-60 per pixel.

2.3 Near-IR spectroscopy with SOAR / TripleSpec4.1

We observed J1144 with TripleSpec4.1 on UT 2022-02-13 under NOIRLab program 2022A-389756 (PI: X. Fan). TripleSpec4.1 utilises a fixed spectroscopic slit of 1.1×28 arcsec and produces cross-dispersed spectra that cover a simultaneous wavelength range from 0.95 to 2.47 microns, at a spectral resolution of ~ 3500.

The observations were performed in three consecutive ABBA patterns, with 40s exposures at each dither position. The detector was read out with 4-pair Fowler sampling (Fowler & Gatley 1990). The seeing was 1 arcsec in *J*-band. Observations of the A0V star, HIP 56984, were obtained immediately prior to J1144 to serve as a telluric and flux standard. The data were processed with the Spextool software package (Cushing et al.

---

[b]See https://wise2.ipac.caltech.edu/docs/release/allwise/expsup/index.html.

[c]But see Bessell (1999) regarding correction of telluric features.
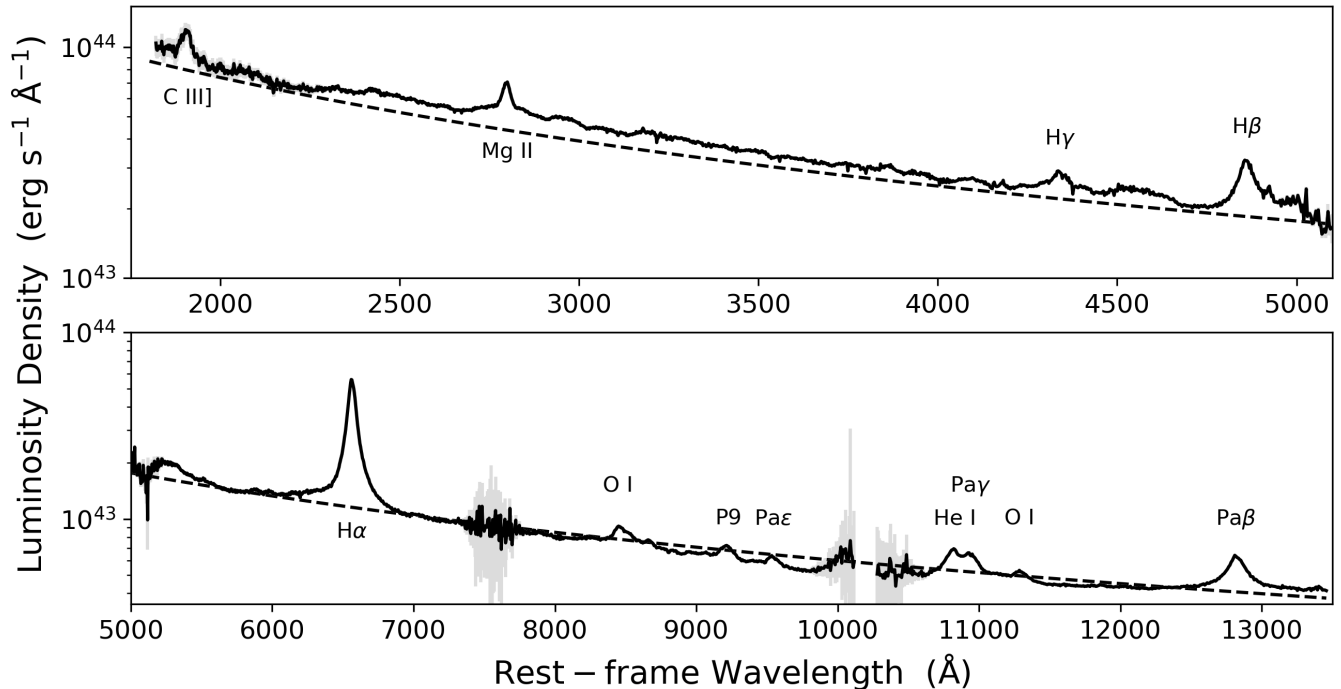[d]Available from https://www.mpe.mpg.de/~ott/QFitsView/

Figure 1. Rest-frame spectrum of J1144, in units of erg s^{-1} Å^{-1}. Uncertainties are shown with grey errorbars, typically smaller than the thickness of the line. The dashed line shows a power-law continuum with slope α_λ=-1.56, which fits the spectrum well up to wavelengths of 7000 Å. The spectrum shown here has been corrected for Galactic reddening, but not for any internal reddening.

2004, 2014) written in the Interactive Data Language (IDL^e), as modified for TripleSpec4.1^f. Telluric correction was applied using the xtellcorr package (Vacca et al. 2003) in IDL. The final S/N was $50 - 100$ per pixel.

3. Spectroscopic analysis

We normalise the spectra by anchoring them to the photometric data which best overlap the cleanest wavelength regions of each spectrum. This involves the g, r, and i bands from SMSS DR3 and the 2MASS H-band for the near-IR spectrum. The bandpass details were retrieved from the Spanish Virtual Observatory (SVO) Filter Profile Service^g (Rodrigo et al. 2012; Rodrigo & Solano 2020). There is good agreement amongst the calibrations provided by the available photometric bands (typically better than 5%), consistent with the small levels of photometric variability discussed in Sec. 4.

We correct for Galactic reddening using the Fitzpatrick et al. (2019) extinction curve, as implemented in the dust_extinction Python package (Gordon 2021). We assume $R_V = 3.1$, and we take the $E(B - V) = 0.123$ mag from Schlegel et al. (1998) and additionally apply the $\times 0.86$ correction factor of Schlafly & Finkbeiner (2011).^{h} The spectra are

combined as the weighted mean on a new wavelength grid which sampled the spectra in pixels at 200 km s^{-1} spacing. The strong emission lines in the J1144 spectrum (Mg II, Hβ, Hα, and Paβ) were used together (weighted mean) to provide a redshift estimate of 0.8314 ± 0.0001. The observed spectrum is then transformed to rest-frame wavelengths and to luminosity in units of erg s^{-1} Å^{-1}, giving a velocity resolution of 109 km s^{-1} pixel^{-1} and a final S/N between 100 and 250 per pixel. The combined spectrum is shown in Figure 1.

When fitting the spectrum, we separately consider the wavelength regimes around C III], Mg II, Hβ, Hα, and Paβ. For each wavelength region, we first fit a combined power-law continuum and iron template. The best power-law slope for the combined UV/optical range is found to be $\alpha_\lambda = -1.56$, although a flatter slope of -0.79 is a better fit for the near-IR, likely reflecting the contributions of hot dust in the region longward of 1 µm (cf. the *WISE* photometry in Fig. 4). Because of the impact of the iron model on the remaining emission line profiles, we test the systematic effects of adopting various iron emission templates in the UV and optical portions of the spectrum. For the UV iron templates, we use those of Shen & Liu (2012, ; implementing a combination of Vestergaard & Wilkes (2001), Tsuzuki et al. (2006), and Salviander et al. (2007)), Tsuzuki et al. (2006), and Mejía-Restrepo et al. (2016), while for the optical templates, we use those of Boroson & Green(1992; BG92, hereafter), Tsuzuki et al. (2006), Bruh-

---

^{e}See https://www.l3harrisgeospatial.com/Software-Technology/IDL.

^{f}See https://noirlab.edu/science/observing-noirlab/observing-ctio/observing-soar/data-reduction/triplespec-data.

^{g}See http://svo2.cab.inta-csic.es/theory/fps/.

^{h}The $E(B - V)$ map recommended by Schröder et al. (2021), from the generalised needlet internal linear combination (GNILC) analysis of the *Planck* 2015 data release Planck Collaboration et al. (2016), gives a consistent value of

0.121 ± 0.004 mag. Schröder et al. (2021) also suggest retaining the rescaling factor of 0.86.

weiler & Verner (2008), and Park et al. (2022). The velocity broadening of the template is a free parameter in each fit. On average, the best-fit iron full width at half-maximum (FWHM) was ~ 2500 km s^{-1}. The systematic errors arising from the iron template choice are square-added to the statistical errors in the fit results below.

For the subsequent steps of the spectral modelling, the emission lines are each fit with a sum of three Gaussian profiles. We estimate the statistical uncertainties on the fit parameters via a Monte Carlo approach, taking the RMS from 50 realisations in which the flux at each pixel is varied according to the error spectrum. Because of the weak [O III] and [S II] emission and lack of evident narrow-line contribution to the Balmer lines, even in the original $R \sim 7000$ spectrum of Hβ, no narrow-line subtraction is performed for the Balmer lines or the [N II] lines near Hα. Integrating $3\times$ the error spectrum over spectral windows of ± 200 km s^{-1} around [O III] 5007 Å and [S II] 6716 + 6731 Å provides conservative upper limits of 5×10^{42} and 3×10^{42} erg s^{-1}, respectively; however, the blending of Hα with [N II] precludes a similar upper limit estimate for the latter.

The emission line fits are shown in Figure 2. The C III] fit is poorly constrained, because of limited wavelength coverage, the lower spectral resolution of the SAAO data from which it is principally observed, and lack of de-blending with Al III and Si III]. As a result, the parameters are omitted from Table 1. The features redward of Hβ are likely iron lines that have not been well modelled because of errors in the flux calibration at the long-wavelength limit of the optical spectra.

From the sum of the Gaussian fits, we determine the velocity shift (derived from the peak of the line profile), the integrated line luminosity, the FWHM, and the second moment of the line profile (σ_{line}). The emission line properties are summarised in Table 1. As was the case for the continuum luminosities, the emission line luminosity errors are dominated by the photometric calibration uncertainties.

Table 1. Emission Line Fit Results

Line	Line Shift[a]	Luminosity	FWHM	σ_{line}
	(km s^{-1})	(10^{44} erg s^{-1})	(km s^{-1})	(km s^{-1})
Mg II	-180 ± 110	6.6 ± 0.9	3100 ± 240	1670 ± 240
Hβ	-120 ± 70	9.0 ± 1.0	3200 ± 240	2750 ± 310
Hα	20 ± 10	46.8 ± 0.8	3390 ± 40	3380 ± 170
Paβ	-10 ± 100	4.2 ± 0.1	3450 ± 60	2890 ± 80

a   Measured with the emission line peak.

3.1 *Luminosity of J1144*

From the power-law continuum fits, we determine the luminosities at several rest-frame wavelengths of interest:
$\log_{10}$ ($\lambda L_\lambda(3000\text{Å})$ / erg s^{-1}) = 47.12 ± 0.04,
$\log_{10}$ ($\lambda L_\lambda(5100\text{Å})$ / erg s^{-1}) = 46.94 ± 0.04, and
$\log_{10}$ ($\lambda L_\lambda(1\mu\text{m})$ / erg s^{-1})   = 46.67 ± 0.04,
where the errors are dominated by the 0.1 mag uncertainties in the flux calibration but do not incorporate the small

additional factor of source variability (see Sec. 4). The luminosity at 3000 Å translates into an absolute magnitude of $M_{300nm} = -28.70$ mag (AB). To aid comparison with higher-redshift samples, we extrapolate the best-fit continuum power-law (with $\alpha_\lambda = -1.56$) to shorter wavelengths and find $\log_{10}$ ($\lambda L_\lambda(1450\text{Å})$ / erg s^{-1}) = 47.2 or M_{145nm} = -28.36 mag (AB). Using the prescription of Richards et al. (2006), we find $M_i(z = 2) = -29.74$ mag (AB).

We adopt the bolometric correction (BC) for 3000 Å from Runnoe et al. (2012b,a), although their BC values for 5100 Å (with spectral slope correction) or the BC values from Netzer (2019) yield similar results. The bolometric luminosity of J1144 is $(4.7 \pm 1.0) \times 10^{47}$ erg s^{-1}, where the uncertainty accounts for the variation arising from different BC assumptions. For the canonical radiative efficiency of 0.1 (e.g., Yu & Tremaine 2002), this equates to an accretion rate of ~ 80 M$_\odot$ yr^{-1}.

3.2 *BH Mass of J1144*

The wide wavelength coverage of our spectroscopic data provides access to several emission lines from the broad line region (BLR), which can be used to estimate the mass of the central BH in J1144 through the virial relations. Anchored to the Hβ reverberation mapping results from the local AGN sample (see Peterson et al. 2004), the virial relations rely on a single epoch of line width and luminosity measurements to infer the velocity of the BLR gas around the BH, as well as the characteristic distance from the BH to the line-emitting gas in question (see, e.g., Cackett et al. 2021, and references therein). Each emission line may have its own velocity and distance, which should yield consistent mass estimates under the assumption that the gravity of the BH dominates the gas dynamics. However, we do note that J1144 represents an extrapolation of a factor of ~ 10 in luminosity compared to the well measured Hβ reverberation mapping sample of Bentz et al. (2013).

We adopt the M_{BH} relation parameters indicated in Table 2 for a functional form of

$$M_{BH} = 10^A \times (FWHM/10^3)^B \times (L_{cont/line}/10^{44})^C \quad (1)$$

for the emission line FWHM in units of km s^{-1}, and the luminosity of either continuum or emission line in units of erg s^{-1}. With the relations being primarily drawn from Le et al. (2020), the A parameters in Table 2 have been renormalised to that paper's adopted virial factor of f = 1.12 (from Woo et al. 2015) for these FWHM-based measurements.

With the emission line measurements of Table 1 and the continuum luminosities indicated above, we derive several complementary BH mass estimates. The M_{BH} values we estimate are presented in Table 3. For Mg II, we do not apply the mass correction factors from Le et al. (2020) for the emission line shape (FWHM/σ_{line} ratio) and spectral slope, which would increase that mass estimate by 0.3 dex and make it more discrepant with the other emission line results. The different emission lines produce BH mass estimates that span the range from $(1.9 - 3.8) \times 10^9$ M$_\odot$. The high S/N of our spectroscopic data mean the statistical errors on the BH mass estimate are small compared to the systematic errors. Dalla Bontà et al.
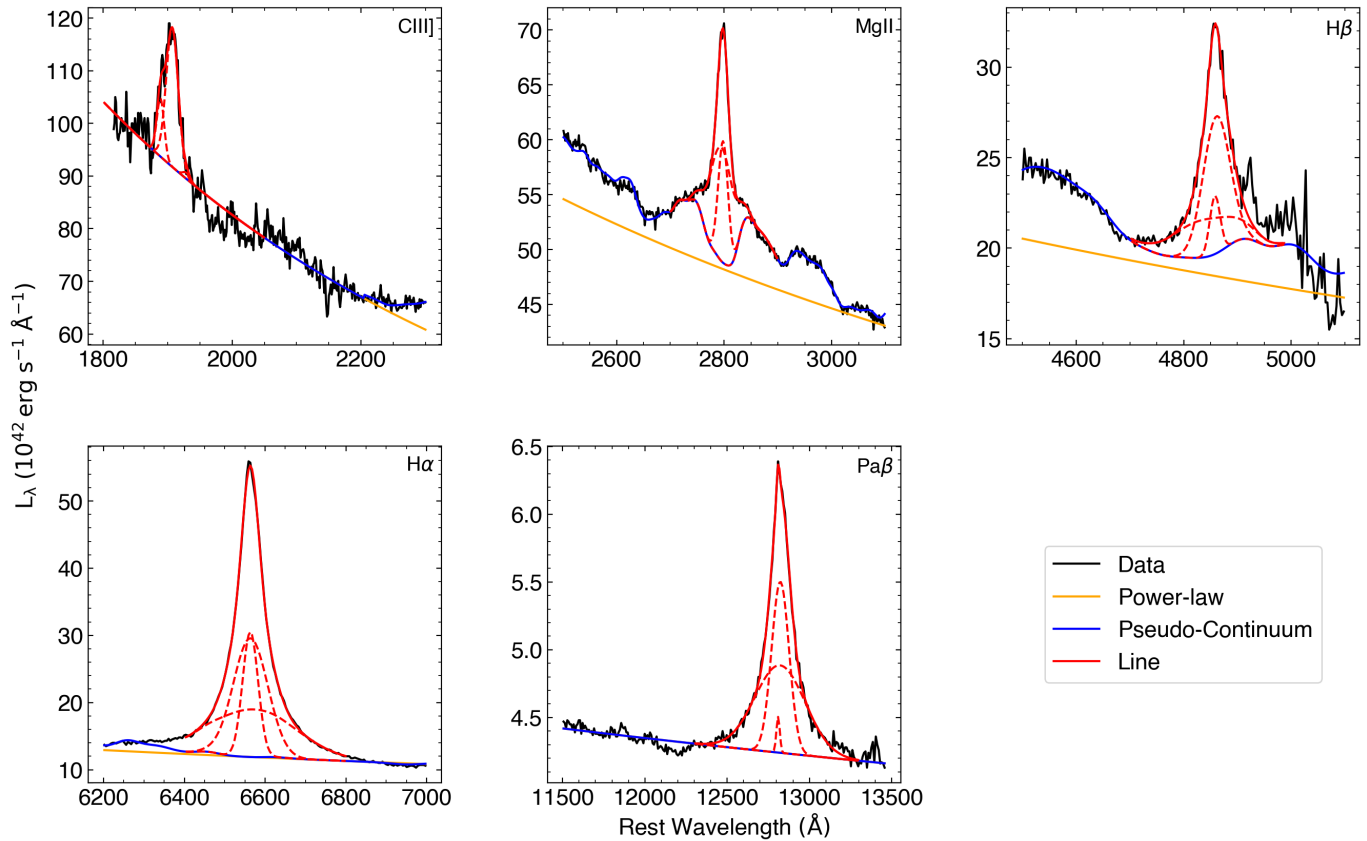
Figure 2. Emission line fits to C III], Mg II, Hβ, Hα, and Paβ, as indicated in each panel. Black lines indicate the data. The model is plotted with progressively added elements: the power-law continuum (orange), then the pseudo-continuum from the broadened iron template (blue), then the emission line fits (red). The red dashed lines indicate the three Gaussian profiles used to fit each line. The particular fits shown here use the Shen & Liu (2012) and BG92 templates in the UV and optical, respectively.

Table 2. Virial Relations

Emission Line	Luminosity (cont/line)	A	B	C	Reference
Mg II	3000 Å	7.04	2.0	0.5	1
Hβ	5100 Å	6.87	2.0	0.533	1
Hβ	Hβ	7.79	2.0	0.54	1
Hα	Hα	7.51	2.06	0.46	2
Paβ	1 μm	7.15	1.76	0.44	3[a]

References: 1 - Le et al. (2020); 2 - Woo et al. (2015); 3 - Landt et al. (2013).
[a] Rescaled from f = 1.4 to f = 1.12.

Table 3. BH Mass Estimates

Emission Line	Luminosity	BH Mass ± Stat. Error (10^9 M$_\odot$)
Mg II	3000 Å	3.83 ± 0.62
Hβ	5100 Å	2.81 ± 0.44
Hβ	Hβ	2.07 ± 0.34
Hα	Hα	2.35 ± 0.06
Paβ	1 μm	1.87 ± 0.09
Combined Estimate ± Sys. Error		**2.6 $^{+5.6}_{-1.8}$**

(2020) estimate the intrinsic scatter to be 0.371 dex for the best-measured FWHM-based virial relation (using Hβ and 5100 Å), and the systematic errors for the other estimates are likely to be larger. Thus, we take the mean value of our five measurements as the best estimate for the BH mass in J1144, M_{BH} = 2.6×10^9 M$_\odot$, and conservatively adopt an uncertainty of 0.5 dex (cf. Vestergaard & Osmer 2009). Our measurements of the bolometric luminosity and BH mass yield an Eddington ratio of ≈ 1.4 for J1144.

In Table 4, we present a summary of the observed and derived properties of J1144.

3.3 Continuum Slope and Internal Reddening

Typical thin disk (Shakura & Sunyaev 1973) and slim disk (Abramowicz et al. 1988) models of BH accretion predict UV/optical continuum emission having a power-law slope of $\alpha_\lambda \approx -2.3$ ($\alpha_\nu \approx +0.3$), though real quasars are rarely observed to be so blue (Xie et al. 2016). Taking such a spectral slope as the limiting case, we can assess the maximum amount of internal reddening that may be present in the emitted spectrum of J1144.

For a UV-flat reddening curve like that of Gaskell & Benker (2007, GB07, hereafter), we find that a maximum intrinsic E(B–V) of 0.17 mag provides a reasonable fit to the

Table 4. Summary of J1144 Properties

Property	Value	Unit	Notes
α (J2000)	176.199041	deg	SMSS DR3
δ (J2000)	−43.149829	deg	SMSS DR3
l	290.222	deg	SMSS DR3
b	+18.071	deg	SMSS DR3
E(B-V)	0.123	mag	[1]
SMSS object_id	84280208	…	DR3
SMSS u	14.974 ± 0.029	mag (AB)	DR3
SMSS v	15.026 ± 0.033	mag (AB)	DR3
SMSS g	14.534 ± 0.014	mag (AB)	DR3
SMSS r	14.424 ± 0.017	mag (AB)	DR3
SMSS i	14.270 ± 0.007	mag (AB)	DR3
SMSS z	14.097 ± 0.006	mag (AB)	DR3
Gaia source_id	5379240246670899584		DR3
Gaia G	14.3887 ± 0.0028	mag (Vega)	DR3
Gaia B_P	14.6397 ± 0.0036	mag (Vega)	DR3
Gaia R_P	13.9321 ± 0.0040	mag (Vega)	DR3
2MASS J	12.806 ± 0.024	mag (Vega)	
2MASS H	12.563 ± 0.022	mag (Vega)	
2MASS K_s	11.877 ± 0.024	mag (Vega)	
WISE $W1$	10.272 ± 0.006	mag (Vega)	AllWISE
WISE $W2$	9.103 ± 0.006	mag (Vega)	AllWISE
WISE $W3$	6.741 ± 0.007	mag (Vega)	AllWISE
WISE $W4$	4.705 ± 0.018	mag (Vega)	AllWISE

Derived Quantities			
Redshift	0.8314 ± 0.0001	…	
M_{BH}	2.6×10^9	$M_\odot$	
$\lambda L_\lambda (3000\text{Å})$	1.3×10^{47}	erg s^{-1}	
$\lambda L_\lambda (5100\text{Å})$	8.7×10^{46}	erg s^{-1}	
$\lambda L_\lambda (1\mu m)$	4.7×10^{46}	erg s^{-1}	
L_{bol}	4.7×10^{47}	erg s^{-1}	
M_{300nm}	−28.70	mag (AB)	
M_{145nm}	−28.36	mag (AB)	
$M_i (z=2)$	−29.74	mag (AB)	
Eddington Ratio	1.4	…	

[1] From Schlegel et al. (1998).

data. In contrast, a UV-steep reddening curve – one lacking the strong bump at 2175 Å – such as the Gordon et al. (2003) model for the star-forming bar of the Small Magellanic Cloud, implies a maximum E(B-V) of 0.10 mag to avoid over-correcting C III], but then under-corrects the spectrum near Mg II. (Reddening curves retaining the 2175 Å bump perform even worse in the regime between C III] and Mg II.) The GB07 reddening correction would lift the 3000 Å luminosity by 0.34 dex, which might be expected to increase each of the BH mass and the Eddington ratio by roughly half that margin. However, because the sources anchoring the virial relations have not been corrected for internal reddening, the appropriate adjustments for J1144 would be reduced in

amplitude.

It is also worth highlighting that the power-law prescription for the rest-frame UV spectrum breaks down in accretion disk models at higher BH masses, as the high-energy turnover migrates to longer wavelengths (e.g., see Campitiello et al. 2018). For $M_{BH} \sim 10^9$ $M_\odot$, the departure from a power-law exceeds 0.1 magnitudes between 2000 and 3000 Å, suggesting extreme care must be taken to disentangle the intrinsic spectral shape from any internal reddening. Observed-frame UV spectroscopy of J1144 should contribute to our ability to remove such degeneracies.

Finally, reddening will lead to an enhancement of the Balmer decrement, i.e., the Hα/Hβ flux ratio. Low-redshift quasars with blue spectral slopes (implying little intrinsic reddening) are often found to have Balmer decrements of 3.1 (Dong et al. 2008). Our observed Balmer decrement of 5.1 would imply E(B-V) ≈ 0.4 mag, depending on the reddening curve adopted. However, Gaskell (2017) has argued that quasar Balmer decrements are consistent with an assumption of intrinsic Case B recombination and a flux ratio of 2.72, which would suggest even more reddening in J1144: E(B-V) ≈ 0.5 mag. In either case, such high reddening appears to be incompatible with the expected spectral slopes, suggesting an intrinsically higher Balmer decrement, which can arise from optical depth effects redistributing Hβ photons into Hα and Paα (Pottasch 1960; Netzer 1975).

4. Ancillary Datasets

The unusually bright nature of J1144 raises the question of whether it has historically been fainter, contributing to its long-standing anonymity.

4.1 Optical data

On UT 1890-05-26, the 8-inch "Bache doublet" telescope at "Mount Harvard" near Chosica, Peru, obtained a 60-minute exposure showing J1144. The photographic glass plate (b5269) has been digitised, and astrometrically and photometrically calibrated by the Digital Access to a Sky Century @ Harvard (DASCH) project[i] (Laycock et al. 2008; Tang et al. 2013). The brightness of J1144 in the 1890 image is estimated to be 14.80 ± 0.16 mag (AB), calibrated to Pan-STARRS g-band using the Asteroid Terrestrial impact Last Alert System (ATLAS) All-Sky Stellar Reference Catalog (Tonry et al. 2018a). Similar plates available through DASCH from more recent epochs show J1144 with estimated g-band magnitudes between 13.9 and 15.1 mag (AB; omitting highly uncertain measurements or those close to the plate's limiting depth). The heterogeneity of the data precludes a more detailed analysis, but the DASCH photographic archives indicate that the optical brightness of J1144 has not varied by more than a factor of ~ 2 in the last 130 years.

Considering data focused on the blue end of the optical spectrum, photographic glass plates taken by the UK Schmidt telescope at SSO on UT 1977-03-21, as part of the ESO/SERC

---

[i]See https://library.cfa.harvard.edu/dasch.

Southern Sky Survey, measured $B_J = 14.7 \pm 0.4$ mag (Vega), as catalogued[j] by the SuperCOSMOS Sky Survey (Hambly et al. 2001b,a). The B_J and SMSS g bandpasses are similar (e.g., see the B_J throughput compared to the Sloan Digital Sky Survey g_{SDSS} in Richards et al. 2005) and the $(B_J - g)$ colours of 3673 quasars in the redshift range $0.6 - 1.0$ from the 2dF and 6dF QSO Redshift Surveys (2QZ/6QZ; Croom et al. 2004) show a median of 0.10 mag with a scaled median absolute deviation (SMAD) of 0.38 mag. With an SMSS DR3 g-band magnitude of 14.534 ± 0.014 mag (AB), we conclude there has been no significant variation in the J1144 brightness at rest-frame ~ 2700 Å compared to 45 years ago.

On more recent timescales, the SMSS DR3 dataset incorporates images of J1144 acquired between February 2015 and June 2018. Across that time window, each of the six SMSS filters shows a brightening of ≈ 0.1 mag, with $7 - 9$ epochs per filter. Denser time sampling is available from the ATLAS telescopes (Tonry et al. 2018b; Smith et al. 2020), which have observed J1144 at a high rate (typically over 200 times per year) since December 2017[k]. Both the o ("orange"; comprising 80% of the data) and c ("cyan") filters show a brightening of 0.2 mag relative to the earliest ATLAS epoch (January 2016), with a peak roughly in May 2020. Together, these datasets provide a consistent picture of modest brightness variations over timescales of days to years.

To probe even shorter timescales, we examined the J1144 data available from two $\sim$month-long visits by the *Transiting Exoplanet Survey Satellite* (*TESS*; Ricker et al. 2015), one beginning on UT 2019-03-26 (during the primary mission; Sector 10) and one beginning on 2021-04-02 (first extended mission; Sector 37). In the *TESS* Input Catalog (TIC; Paegert et al. 2022), J1144 has the designation TIC 61537875, but it was not selected for the Candidate Target List. As a result, photometry is only available from the Full Frame Image (FFI) dataset, which were acquired every 30 minutes in the primary mission and every 10 minutes in the first extended mission. The coarse spatial resolution of *TESS* results in J1144 being heavily blended with TIC 61537878, a star 30 arcsec away that is ~ 1 mag brighter in *TESS*'s wide bandpass ($600 - 1000$ nm). As a result, precise photometry is difficult to obtain, but we note no significant fluctuations above 1% in the combined light curve of the quasar and star.

4.2 IR data

Turning to the IR, the NEOWISE 2022 Data Release[l] (Mainzer et al. 2014) provides $W1$ and $W2$ photometry for J1144 at more than 250 epochs between UT 2014-01-09 and 2021-06-19. At rest-frame equivalents of 1.8 and 2.5 μm for $W1$ and $W2$, respectively, the *WISE* data is dominated by the hot dust near the quasar, rather than the quasar's accretion disk that is probed at shorter wavelengths. In Figure 3, we show the *WISE* and ATLAS light curves, binned to 30-day median values.

[j]See http://www-wfau.roe.ac.uk/sss/index.html.
[k]See https://fallingstar-data.com/forcedphot/.
[l]See https://wise2.ipac.caltech.edu/docs/release/neowise/.
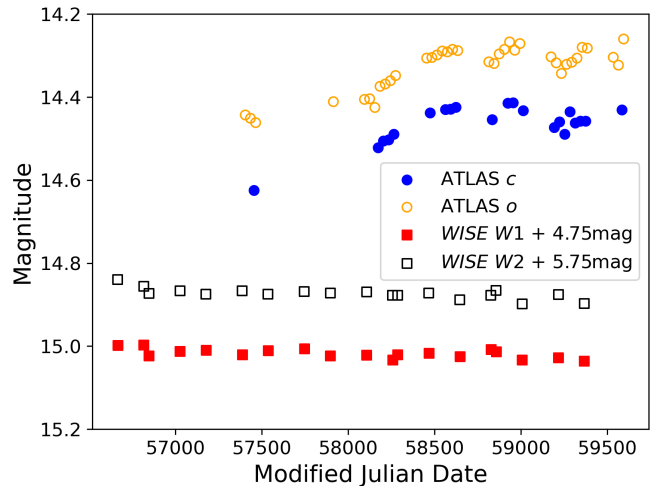
Figure 3. ATLAS and *WISE* light curves for J1144 over the past 8 years. Photometry was binned to 30-day median values for each bandpass. The ATLAS photometry is in AB magnitudes, while the the IR photometry is in Vega magnitudes and has been shifted vertically for convenience. Any increase in the optical brightness would take a decade to be reflected in the dust luminosity because of the large dust sublimation region around luminous quasars like J1144.

In contrast to the ATLAS photometry, J1144 exhibits a very slight fading in both IR bands over that time period, with an amplitude of ~ 0.05 mag, comparable to the level of intraday photometric scatter. This uncorrelated behaviour can be understood in the context of the multi-year time lags for dust reverberation that would be expected from the large dust sublimation radius implied by the high luminosity of J1144. For the luminosity of J1144 (1.2×10^{14} L$_\odot$), the predicted time lag for the IR response to optical variations would be 9.7 years (Lyu et al. 2019), slightly longer than the time span shown in Figure 3. Thus, the steadiness of the IR photometry since the start of *WISE* operations implies no significant and lengthy changes in the quasar luminosity over the past $\sim$20 years.

As the recent increase in luminosity shown by the ATLAS light curves propagates into the dust surrounding the quasar, we could expect to see the IR similarly brighten within the next decade. However, the relative amplitude of IR variability in response to optical fluctuations is extremely broad, between factors of 0.1 and 10 for high-luminosity, high-time-lag sources (Lyu et al. 2019, cf. their Fig. 14). Future monitoring by *WISE* and the Dynamic REd All-sky Monitoring Survey (DREAMS; Soon et al. 2020) may reveal the amplitude of the dust response in J1144.

4.3 X-ray data

In X-rays, there are no point-source counterparts to J1144 catalogued in the Second *ROSAT* all-sky X-ray Survey (2RXS; Boller et al. 2016). Cross-matching confirmed quasars from Milliquas, approximately 75% of the *Gaia G* < 16 mag (Vega) quasars in the redshift range $z = 0.7 - 0.9$ have 2RXS counterparts. For our extinction-corrected 2500 Å flux of $F_\nu = 3.8 \times 10^{-26}$ erg s^{-1} cm^{-2} Hz^{-1}, we would expect a 2 keV X-ray

flux of $\sim 2 \times 10^{-30}$ erg s^{-1} cm^{-2} Hz^{-1} (Bisogni et al. 2021), roughly a factor of 10 greater than the nominal 2RXS flux limit (Boller et al. 2016). Whether the non-detection is an indication of intrinsic X-ray weakness or absorption (local to the quasar or intervening) may be clarified by forthcoming data releases from *SRG/eROSITA* (the *Spectrum-Roentgen-Gamma* satellite's *extended ROentgen Survey with an Imaging Telescope Array*; Predehl et al. 2021).

4.4 Radio data

The closest radio detection in DR1 of the Rapid ASKAP Continuum Survey[m] (RACS; McConnell et al. 2020; Hale et al. 2021) is 48 arcsec from J1144, which at $z = 0.83$ corresponds to more than 350 kpc projected distance. If we assume an association between J1144 and RACS-DR1 J114451.8-430920, then the flux density of 5.1 ± 0.5 mJy at 887.5 MHz implies a rest-frame 5 GHz luminosity density of 7.6×10^{31} erg s^{-1} Hz^{-1} (for a spectral index of $\nu^{-0.6}$). For an optical (rest-frame 4400 Å) luminosity density of 1.4×10^{32} erg s^{-1} Hz^{-1} (derived from the global power-law continuum shown in Figure 1), this gives an upper limit to the radio-loudness (using the definition of Kellermann et al. 1989) of $R < 0.54$. Thus, even a putative association[n] between the RACS DR1 source and J1144 leaves the quasar in the radio-quiet regime.

The absence of strong X-ray and radio emission, in conjunction with the low levels of UV-to-IR variability, make it unlikely for J1144 to have a relativistically beamed jet. Thus, we conclude that J1144 is not a blazar.

4.5 On the possibility of gravitational lensing

Given the high luminosity, it is natural to wonder if the source is gravitationally lensed (e.g., Fan et al. 2019). To check for a small-separation galaxy lens, we examine the corrected B_P and R_P flux excess, C^*, from *Gaia* EDR3 (Riello et al. 2021), which makes a standardised comparison between the flux measured in the 0.35-arcsec-wide G-band photometric aperture with the integrated fluxes measured in the 3.5-arcsec-wide apertures for the B_P and R_P photometry (integrating along the wavelength dimension of the low-resolution spectra). With $C^* = 0.023$, the variation in flux measured by the different extraction apertures for the *Gaia* photometry is within 2σ of the 0-value expected for point sources of the brightness of J1144 (where $\sigma = 0.012$). Amongst the small-separation gravitationally lensed quasars[o] that are associated with a single *Gaia* EDR3 source, Q1208+101 has the smallest C^* value at

0.168, a factor of 7 times larger than J1144. Similarly, the G-band variability proxy of Mowlavi et al. (2021) has a value of 0.015, suggesting that the *Gaia* small-aperture measurements across a range of scan directions have found peak-to-peak flux variations of ~ 0.05 mag (cf. their Sect. 3).

While we conclude that there is no indication of gravitational lensing for J1144 in the existing *Gaia* data, the lack of microlensing-induced flux variations evident in the recent photometric sampling described above cannot fully exclude the existence of a lensing galaxy, as Mosquera & Kochanek (2011) found that roughly half of lensed quasars are likely to be in a "demagnified valley" in any given 10-year period. Thus, a high-spatial-resolution imaging study of J1144 would be of great interest.

5. Comparison with other bright quasars

As the single brightest quasar in the sky, 3C 273 is an important benchmark for luminous quasars, as its long observational history and low redshift have made it a forefront laboratory for exploring accretion processes (e.g., Courvoisier 1998; Gravity Collaboration et al. 2018). Moreover, the presence of the strong radio jet, with synchrotron emission that extends into the optical regime, has opened a window into the relatively rare class of radio-loud quasars (e.g., Bahcall et al. 1995; Jester et al. 2005; Uchiyama et al. 2006).

In Figure 4, we compare the rest-frame UV-to-IR spectral energy distribution (SED) of J1144 from recent data to the minimum and maximum luminosities of 3C 273 (including synchrotron flares), as observed over a 40-year span[p] (Türler et al. 1999; Soldi et al. 2008), as well as to SMSS J2157-3602, the most luminous known quasar in the Universe, at a redshift of $z = 4.692$ (Wolf et al. 2018a; Onken et al. 2020). The J1144 SED is derived from a subset of the photometry presented in Table 4, namely, that of SMSS DR3 (u, v, g, r, i, z), 2MASS (J, H, K)[q], and AllWISE ($W1, W2, W3, W4$). The photometry in Figure 4 was corrected for Galactic extinction up to an observed-frame wavelength of 3 μm using the Fitzpatrick et al. (2019) extinction curve, a standard R_V=3.1 Milky Way dust model, and the Schlegel et al. (1998) E(B-V) values of 0.123, 0.021, and 0.015 mag for J1144, 3C 273, and SMSS J2157, respectively, with the $\times$0.86 correction factor of Schlafly & Finkbeiner (2011). As with the spectroscopic calibration above, the bandpass details were retrieved from the SVO. The SMSS u- and v-band photometry were also corrected with the stellar-colour regression method of Huang et al. (2021), which makes them 0.088 and 0.069 mag fainter, respectively. (The corrections for g- and r-band are less than 0.01 mag and are therefore omitted.)

Across the entire observed UV/optical range, J1144 has an intrinsic luminosity that is roughly 8 times greater than the brightest observations of 3C 273, and only about 3 times

---

[m]See the interactive Hierarchical Image Survey (HiPS) map in the Aladin sky atlas (Bonnarel et al. 2000) under "Collections-Image-Radio-RACS".

[n]We further caution the reader that the visual appearance of this RACS source is plausibly of a core and (low-significance) two-lobe structure unassociated with J1144, but without any detected counterpart in SMSS DR3, VHS, or unWISE. Deeper i- and z-band images from the DECam instrument (Flaugher et al. 2015) on the CTIO 4m telescope, taken as part of programs 2017A-0260 (PI: M. Soares-Santos) and 2019A-0272 (PI: A. Zenteno), do not reveal any sources aligned with the centre of the radio "core".

[o]We utilise the catalogue at https://research.ast.cam.ac.uk/lensedquasars/ compiled by C. Lemon.

[p]Data retrieved from the INTEGRAL Science Data Centre (ISDC): http://isdc.unige.ch/3c273/.

[q]The J and K_s photometry available from DR6 of the VISTA Hemisphere Survey (McMahon et al. 2013) is little different from the 2MASS data of ~ 20 years earlier.

less than the most luminous quasar known. Even with the occasional synchrotron flares elevating the peak luminosities of 3C 273 in the IR, the blazar has remained $\sim 5\times$ less luminous than J1144. The inset in Figure 4 includes the maximum potential radio luminosity observed for J1144, on the assumption of the RACS DR1 detection being associated with the quasar, illustrating the dramatic difference in the long–wavelength SED of radio-quiet quasars compared to radio-loud sources such as 3C 273.

In Figure 4, we also show three SED templates[r] (Lyu et al. 2017) exhibiting different mid-IR dust properties. The "Normal SED" represents the typical broad-line quasar SED, while the hot-dust-deficient (HDD) and warm-dust-deficient (WDD) templates show reduced emission at shorter and longer mid-IR wavelengths, respectively. With the templates anchored to match the J1144 SED near 1 μm, the *WISE* photometry suggests that J1144 is an intermediate case and may be somewhat lacking in dust close to the quasar.

In addition, we note the similarity between the optical spectra of J1144 (Fig. 1 and 2) and 3C 273 (Dietrich et al. 1999), with prominent Balmer lines and comparatively weak [O III] emission, suggesting a commonality in their central engines despite the differences in their radio properties. Compared to the sample of bright quasars analysed by BG92, J1144 is on the strong Fe II–weak [O III] end of their "Eigenvector 1" correlation, although the Fe II equivalent width[s] (EW) of $\sim$ 40 Å is typical of radio-quiet quasars. The ratio of Fe II-to-Hβ EWs of 1.5 is at the high end of their distribution, but J1144 does not exhibit the enhanced blue Hβ asymmetry often seen for such sources.

In Figure 5, we compare the J1144 bolometric luminosity estimated in Section 3.1 to 3C 273, SMSS J2157, and a large number of quasars, drawn from either the SDSS DR14 quasar catalogue (DR14Q; Rakshit et al. 2020) or Milliquas, as a function of lookback time. In order to use a consistent bolometric correction, we estimate the continuum luminosities at 3000 Å for the literature sources. For 3C 273, we use the mean *U*-band flux from the 40-year dataset of the ISDC. DR14Q values use the 3000 Å luminosity tabulated in the catalogue, or, at higher or lower redshifts, respectively, estimate $\log_{10}\left(\lambda L_\lambda(3000)\right)$ from the 1350 Å luminosity as $4.887 + 0.89 \log_{10}\left(\lambda L_\lambda(1350)\right)$ or from the 5100 Å luminosity as $9.213 + 0.792 \log_{10}\left(\lambda L_\lambda(5100)\right)$, based on the best–fit relations from the DR14Q sources having both luminosities estimated. Sources with non-zero QUALITY_L3000 values were excluded. The varied literature sources compiled in Milliquas were cross-matched to the *Gaia* catalogue and an empirical scaling from the R_p photometry to the 3000 Å luminosity as a function of redshift was applied[t]. The Milli-

[r]Retrieved from https://github.com/karlan/AGN_templates.
[s]We adopt the BG92 method of measuring the Fe II flux between 4434 and 4684 Å.
[t]From the *Gaia* photometry of DR14Q sources, we estimated a conversion of $\log_{10}\left(\lambda L_\lambda(3000)\right) = -0.4 R_p + (52.9 + 3 \log_{10}(z) - 0.2z)$ for redshift, z. The scaled median absolute deviation (SMAD) of this relation is 0.133 dex, with a median offset of 0.002 dex.
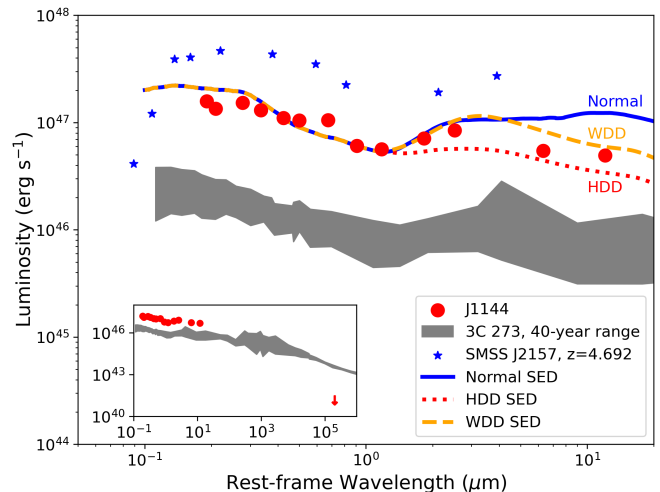
Figure 4. Rest-frame SED for J1144 (red circles) compared to the 40-year range of luminosities of 3C 273 (grey shaded region) from Soldi et al. (2008), and to SMSS J2157 (blue stars), the most luminous known quasar. All three sources have been corrected for Galactic extinction. Single-epoch uncertainties for the J1144 photometry are smaller than the symbols. Three quasar templates from Lyu et al. (2017) are also shown: normal (solid), hot-dust-deficient (HDD; dotted), and warm-dust-deficient (WDD; dashed). The inset shows an expanded range in order to include the potential J1144 radio association from RACS DR1 as an upper limit (arrow) and to indicate the difference in long-wavelength slope from radio-loud quasars like 3C 273.

quas sample has been restricted to sources with spectroscopic redshifts; cleaned of lensed sources, blazars, and a few spurious objects (including those with > 3σ parallax or proper motion estimates); and has omitted quasars from SDSS (to avoid duplication). Beyond z = 5.5, very few Milliquas sources have *Gaia* photometry.

As can be seen from Figure 5, J1144 is the most luminous known quasar out to z = 1.29, a lookback time of 8.7 Gyr, beyond which the quasar, HS 2154+2228 (Hagen et al. 1999), is the first of a small sample of quasars found to be more luminous, up to the pinnacle of SMSS J2157. With an extinction-corrected *i*-band magnitude of 14.059 mag (AB), J1144 is nearly 1 full magnitude brighter than the SDSS cut-off at $i_{\rm SDSS}$ = 15 mag (AB) and nearly 1.5 mag brighter in $M_i(z = 2)$ than any source actually found in the SDSS DR3 quasar luminosity function at redshifts below z = 0.9 (Richards et al. 2006).

6. Discussion

The location of J1144 falls within a small gap in the *GALEX* All-Sky Imaging Survey (AIS; Martin et al. 2005), which explains why it did not appear in DR1 of the UVQS (Monroe et al. 2016). Utilising $\sim 3,000$ known quasars from Milliquas in the same redshift range as J1144, for which both *GALEX* and *Gaia* photometry exist, we use the $FUV - G$ and $NUV - G$ colours to predict J1144 to have (FUV, NUV) = (17, 16) mag (AB), with uncertainties of roughly 1 mag in each band. With FUV = 17 mag (AB), J1144 would have been amongst the top 10% of the brightest discoveries by UVQS DR1, but at a redshift 0.2 higher than the rest.

Figure 5. Bolometric luminosity of J1144 (large red point), 3C 273 (grey square), and SMSS J2157 (blue star), compared to sources from the SDSS DR14 quasar catalogue (DR14Q; black points; Rakshit et al. 2020) and Milliquas (MQ; green points), shown as a function of lookback time (bottom axis) and redshift (top axis). No known quasars are as luminous as J1144 in the last 9 Gyr, and J1144 is only a factor of 2 dimmer than the most luminous known quasar, SMSS J2157.

The high luminosity of J1144 also implies a large size for its BLR. Extrapolating the radius–luminosity relation of Bentz et al. (2013) to the 5100 Å luminosity of J1144 suggests an Hβ-emitting size of $\sim$ 1200 light-days. With the additional time-dilation factor of $\sim$ 2, a reverberation mapping campaign would be a long-term endeavour. However, the angular size of the BLR is expected to be in excess of 100 microarcseconds. Since J1144 has a *K*-band magnitude of 11.9 mag (Vega), its BLR will be well within the reach of the upgraded GRAVITY+ instrument[u] at ESO's Very Large Telescopes. Thus, it may be possible to measure the Paβ dynamics in J1144, comparable to the Paα measurement for 3C 273 (Gravity Collaboration et al. 2018).

Additional studies may make productive use of an exceptionally bright quasar like J1144 as a background source. For example, UV spectroscopy of J1144 may probe the Milky Way's circumgalactic medium (Tumlinson et al. 2017; Zheng et al. 2019; Bish et al. 2021).

Previous searches for quasars and other blue objects in the Southern hemisphere have usually not reached as close to the Galactic Plane as J1144, which lies at *b* = +18.1°. For example, the Edinburgh–Cape Blue Object Survey (Stobie et al. 1997; Kilkenny et al. 2016) was restricted to |*b*| > 30°; the Hamburg/ESO quasar survey (Wisotzki et al. 1996, 2000) searched at |*b*| > 25°; and the Calán–Tololo Survey (Maza et al. 1988, 1996) observed to |*b*| > 20°. Dedicated quasar searches closer to the Galactic Plane (e.g., Im et al. 2007; Fu et al. 2021) may produce samples of objects useful both in their own right and for studies of the gas and dust near the Galactic disk.

Moreover, the discovery power inherent in the recent generation of all-sky surveys like those of *Gaia*, *WISE*, and

eROSITA motivate a fresh examination of what other bright quasars may have been missed in previous searches across the celestial sphere. A spectroscopic campaign underway at the ANU 2.3m telescope has already identified $\sim$ 80 new, bright quasars (in addition to J1144), some with Galactic latitudes in excess of 60 deg. Thus, after 60 years, it would appear we are finally approaching a complete census of bright quasars, with only the discovery of Changing Look Quasars (CLQ; e.g., LaMassa et al. 2015) from forthcoming surveys likely to add to the sample.

---

[u]See https://www.mpe.mpg.de/ir/gravityplus.

in the *Gaia* Multilateral Agreement.

References

Abramowicz, M. A., Czerny, B., Lasota, J. P., & Szuszkiewicz, E. 1988, ApJ, 332, 646

Astropy Collaboration, Price-Whelan, A. M., Sipőcz, B. M., et al. 2018, AJ, 156, 123

Astropy Collaboration, Robitaille, T. P., Tollerud, E. J., et al. 2013, A&A, 558, A33

Bahcall, J. N., Kirhakos, S., Schneider, D. P., et al. 1995, ApJ, 452, L91

Bentz, M. C., Denney, K. D., Grier, C. J., et al. 2013, ApJ, 767, 149

Bessell, M. S. 1999, PASP, 111, 1426

Bish, H. V., Werk, J. K., Peek, J., Zheng, Y., & Putman, M. 2021, ApJ, 912, 8

Bisogni, S., Lusso, E., Civano, F., et al. 2021, A&A, 655, A109

Boller, T., Freyberg, M. J., Trümper, J., et al. 2016, A&A, 588, A103

Bonnarel, F., Fernique, P., Bienaymé, O., et al. 2000, A&AS, 143, 33

Boroson, T. A. & Green, R. F. 1992, ApJS, 80, 109

Brasseur, C. E., Phillip, C., Fleming, S. W., Mullally, S. E., & White, R. L. 2019, Astrocut: Tools for creating cutouts of TESS images

Bruhweiler, F. & Verner, E. 2008, ApJ, 675, 83

Cackett, E. M., Bentz, M. C., & Kara, E. 2021, iScience, 24, 102557

Campitiello, S., Ghisellini, G., Sbarrato, T., & Calderone, G. 2018, A&A, 612, A59

Childress, M. J., Vogt, F. P. A., Nielsen, J., & Sharp, R. G. 2014, Ap&SS, 349, 617

Courvoisier, T. J. L. 1998, A&A Rev., 9, 1

Crause, L. A., Gilbank, D., Gend, C. v., et al. 2019, Journal of Astronomical Telescopes, Instruments, and Systems, 5, 024007

Croom, S. M., Smith, R. J., Boyle, B. J., et al. 2004, MNRAS, 349, 1397

Cross, N. J. G., Collins, R. S., Mann, R. G., et al. 2012, A&A, 548, A119

Cushing, M., Vacca, B., & Rayner, J. 2014, Spextool: Spectral EXtraction tool

Cushing, M. C., Vacca, W. D., & Rayner, J. T. 2004, PASP, 116, 362

Dalla Bontà, E., Peterson, B. M., Bentz, M. C., et al. 2020, ApJ, 903, 112

Dietrich, M., Wagner, S. J., Courvoisier, T. J. L., Bock, H., & North, P. 1999, A&A, 351, 31

Dong, X., Wang, T., Wang, J., et al. 2008, MNRAS, 383, 581

Dopita, M., Hart, J., McGregor, P., et al. 2007, Ap&SS, 310, 255

Dopita, M., Rhee, J., Farage, C., et al. 2010, Ap&SS, 327, 245

Edelson, R. & Malkan, M. 2012, ApJ, 751, 52

Fan, X., Wang, F., Yang, J., et al. 2019, ApJ, 870, L11

Fitzpatrick, E. L., Massa, D., Gordon, K. D., Bohlin, R., & Clayton, G. C. 2019, ApJ, 886, 108

Flaugher, B., Diehl, H. T., Honscheid, K., et al. 2015, AJ, 150, 150

Flesch, E. W. 2021, arXiv e-prints, arXiv:2105.12985

Fowler, A. M. & Gatley, I. 1990, ApJ, 353, L33

Fu, Y., Wu, X.-B., Yang, Q., et al. 2021, ApJS, 254, 6

Gaia Collaboration. 2018, A&A, 616, A1

Gaia Collaboration & et al. 2016, A&A, 595, A1

Gaskell, C. M. 2017, MNRAS, 467, 226

Gaskell, C. M. & Benker, A. J. 2007, arXiv e-prints, arXiv:0711.1013

Ginsburg, A., Sipőcz, B. M., Brasseur, C. E., et al. 2019, AJ, 157, 98

Gordon, K. 2021, karllark/dust_extinction: interstellar dust extinction curves, Zenodo

Gordon, K. D., Clayton, G. C., Misselt, K. A., Landolt, A. U., & Wolff, M. J. 2003, ApJ, 594, 279

Gravity Collaboration, Sturm, E., Dexter, J., et al. 2018, Nature, 563, 657

Greenstein, J. L. 1963, Nature, 197, 1041

Hagen, H. J., Engels, D., & Reimers, D. 1999, A&AS, 134, 483

Hale, C. L., McConnell, D., Thomson, A. J. M., et al. 2021, PASA, 38, e058

Hambly, N. C., Collins, R. S., Cross, N. J. G., et al. 2008, MNRAS, 384, 637

Hambly, N. C., Irwin, M. J., & MacGillivray, H. T. 2001a, MNRAS, 326, 1295

Hambly, N. C., MacGillivray, H. T., Read, M. A., et al. 2001b, MNRAS, 326, 1279

Hamuy, M., Suntzeff, N. B., Heathcote, S. R., et al. 1994, PASP, 106, 566

Heap, S. R. & Lindler, D. 2010, in American Astronomical Society Meeting Abstracts, Vol. 215, American Astronomical Society Meeting Abstracts #215, 463.02

Huang, Y., Yuan, H., Li, C., et al. 2021, ApJ, 907, 68

Im, M., Lee, I., Cho, Y., et al. 2007, ApJ, 664, 64

Irwin, M. J., Lewis, J., Hodgkin, S., et al. 2004, in Society of Photo-Optical Instrumentation Engineers (SPIE) Conference Series, Vol. 5493, Optimizing Scientific Return for Astronomy through Information Technologies, ed. P. J. Quinn & A. Bridger, 411–422

Jester, S., Röser, H. J., Meisenheimer, K., & Perley, R. 2005, A&A, 431, 477

Kellermann, K. I., Sramek, R., Schmidt, M., Shaffer, D. B., & Green, R. 1989, AJ, 98, 1195

Kilkenny, D., Worters, H. L., O'Donoghue, D., et al. 2016, MNRAS, 459, 4343

LaMassa, S. M., Cales, S., Moran, E. C., et al. 2015, ApJ, 800, 144

Landt, H., Ward, M. J., Peterson, B. M., et al. 2013, MNRAS, 432, 113

Laycock, S., Tang, S., Grindlay, J., et al. 2008, arXiv e-prints, arXiv:0811.2005

Le, H. A. N., Woo, J.-H., & Xue, Y. 2020, ApJ, 901, 35

Lightkurve Collaboration, Cardoso, J. V. d. M., Hedges, C., et al. 2018, Lightkurve: Kepler and TESS time series analysis in Python, Astrophysics Source Code Library

Lucy, A. B. 2021, The Detection and Description of Symbiotic Accretion From Cool Evolved Stars, PhD thesis, Columbia University

Lyu, J., Rieke, G. H., & Shi, Y. 2017, ApJ, 835, 257

Lyu, J., Rieke, G. H., & Smith, P. S. 2019, ApJ, 886, 33

Mainzer, A., Bauer, J., Cutri, R. M., et al. 2014, ApJ, 792, 30

Mainzer, A., Bauer, J., Grav, T., et al. 2011, ApJ, 731, 53

Margon, B., Prochaska, J. X., Tejos, N., & Monroe, T. 2016, PASP, 128, 024201

Martin, D. C., Fanson, J., Schiminovich, D., et al. 2005, ApJ, 619, L1

Maza, J., Ruiz, M. T., Gonzalez, L. E., & Wischnjewski, M. 1988, in Astronomical Society of the Pacific Conference Series, Vol. 1, Progress and Opportunities in Southern Hemisphere Optical Astronomy. The CTIO 25th Anniversary Symposium, ed. V. M. Blanco & M. M. Phillips, 410

Maza, J., Wischnjewsky, M., & Antezana, R. 1996, Rev. Mexicana Astron. Astrofis., 32, 35

McConnell, D., Hale, C. L., Lenc, E., et al. 2020, PASA, 37, e048

McMahon, R. G., Banerji, M., Gonzalez, E., et al. 2013, The Messenger, 154, 35

Mejía-Restrepo, J. E., Trakhtenbrot, B., Lira, P., Netzer, H., & Capellupo, D. M. 2016, MNRAS, 460, 187

Monroe, T. R., Prochaska, J. X., Tejos, N., et al. 2016, AJ, 152, 25

Mosquera, A. M. & Kochanek, C. S. 2011, ApJ, 738, 96

Mowlavi, N., Rimoldini, L., Evans, D. W., et al. 2021, A&A, 648, A44

Netzer, H. 1975, MNRAS, 171, 395

Netzer, H. 2019, MNRAS, 488, 5185

Oke, J. B. 1963, Nature, 197, 1040

Onken, C. A., Bian, F., Fan, X., et al. 2020, MNRAS, 496, 2309

Onken, C. A., Wolf, C., Bessell, M. S., et al. 2019, PASA, 36, e033

Paegert, M., Stassun, K. G., Collins, K. A., et al. 2022, VizieR Online Data Catalog, IV/39

Park, D., Barth, A. J., Ho, L. C., & Laor, A. 2022, ApJS, 258, 38

Peterson, B. M., Ferrarese, L., Gilbert, K. M., et al. 2004, ApJ, 613, 682

Planck Collaboration, Aghanim, N., Ashdown, M., et al. 2016, A&A, 596, A109

Pottasch, S. R. 1960, ApJ, 131, 202

Predehl, P., Andritschke, R., Arefiev, V., et al. 2021, A&A, 647, A1

Rakshit, S., Stalin, C. S., & Kotilainen, J. 2020, ApJS, 249, 17

Richards, G. T., Croom, S. M., Anderson, S. F., et al. 2005, MNRAS, 360, 839

Richards, G. T., Strauss, M. A., Fan, X., et al. 2006, AJ, 131, 2766

Ricker, G. R., Winn, J. N., Vanderspek, R., et al. 2015, Journal of Astronomical Telescopes, Instruments, and Systems, 1, 014003

Riello, M., De Angeli, F., Evans, D. W., et al. 2021, A&A, 649, A3

Rodrigo, C. & Solano, E. 2020, in XIV.0 Scientific Meeting (virtual) of the Spanish Astronomical Society, 182

Rodrigo, C., Solano, E., & Bayo, A. 2012, SVO Filter Profile Service Version 1.0, IVOA Working Draft 15 October 2012

Runnoe, J. C., Brotherton, M. S., & Shang, Z. 2012a, MNRAS, 427, 1800

Runnoe, J. C., Brotherton, M. S., & Shang, Z. 2012b, MNRAS, 422, 478

Salviander, S., Shields, G. A., Gebhardt, K., & Bonning, E. W. 2007, ApJ, 662, 131

Sandage, A. 1965, ApJ, 141, 1560

Schlafly, E. F. & Finkbeiner, D. P. 2011, ApJ, 737, 103

Schlafly, E. F., Meisner, A. M., & Green, G. M. 2019, ApJS, 240, 30

Schlawin, E., Herter, T. L., Henderson, C., et al. 2014, in Society of Photo-Optical Instrumentation Engineers (SPIE) Conference Series, Vol. 9147, Ground-based and Airborne Instrumentation for Astronomy V, ed. S. K. Ramsay, I. S. McLean, & H. Takami, 91472H

Schlegel, D. J., Finkbeiner, D. P., & Davis, M. 1998, ApJ, 500, 525

Schmidt, M. 1963, Nature, 197, 1040

Schmidt, M. 1965, ApJ, 141, 1295

Schröder, A. C., van Driel, W., & Kraan-Korteweg, R. C. 2021, MNRAS, 503, 5351

Secrest, N. J., Dudik, R. P., Dorland, B. N., et al. 2015, ApJS, 221, 12

Shakura, N. I. & Sunyaev, R. A. 1973, A&A, 24, 337

Shen, Y. & Liu, X. 2012, ApJ, 753, 125

Shu, Y., Koposov, S. E., Evans, N. W., et al. 2019, MNRAS, 489, 4741

Skrutskie, M. F., Cutri, R. M., Stiening, R., et al. 2006, AJ, 131, 1163

Smith, K. W., Smartt, S. J., Young, D. R., et al. 2020, PASP, 132, 085002

Soldi, S., Türler, M., Paltani, S., et al. 2008, A&A, 486, 411

Soon, J., Adams, D., De, K., et al. 2020, in Society of Photo-Optical Instrumentation Engineers (SPIE) Conference Series, Vol. 11203, Advances in Optical Astronomical Instrumentation 2019, 1120307

Stobie, R. S., Kilkenny, D., O'Donoghue, D., et al. 1997, MNRAS, 287, 848

Tang, S., Grindlay, J., Los, E., & Servillat, M. 2013, PASP, 125, 857

Tody, D. 1986, in Society of Photo-Optical Instrumentation Engineers (SPIE) Conference Series, Vol. 627, Instrumentation in astronomy VI, ed. D. L. Crawford, 733

Tonry, J. L., Denneau, L., Flewelling, H., et al. 2018a, ApJ, 867, 105

Tonry, J. L., Denneau, L., Heinze, A. N., et al. 2018b, PASP, 130, 064505

Tsuzuki, Y., Kawara, K., Yoshii, Y., et al. 2006, ApJ, 650, 57

Tumlinson, J., Peeples, M. S., & Werk, J. K. 2017, ARA&A, 55, 389

Türler, M., Paltani, S., Courvoisier, T. J. L., et al. 1999, A&AS, 134, 89

Uchiyama, Y., Urry, C. M., Cheung, C. C., et al. 2006, ApJ, 648, 910

Vacca, W. D., Cushing, M. C., & Rayner, J. T. 2003, PASP, 115, 389

Vestergaard, M. & Osmer, P. S. 2009, ApJ, 699, 800

Vestergaard, M. & Wilkes, B. J. 2001, ApJS, 134, 1

Wenger, M., Ochsenbein, F., Egret, D., et al. 2000, A&AS, 143, 9

Wisotzki, L., Christlieb, N., Bade, N., et al. 2000, A&A, 358, 77

Wisotzki, L., Koehler, T., Groote, D., & Reimers, D. 1996, A&AS, 115, 227

Wolf, C., Bian, F., Onken, C. A., et al. 2018a, PASA, 35, e024

Wolf, C., Onken, C. A., Luvaul, L. C., et al. 2018b, PASA, 35, e010

Woo, J.-H., Yoon, Y., Park, S., Park, D., & Kim, S. C. 2015, ApJ, 801, 38

Wright, E. L., Eisenhardt, P. R. M., Mainzer, A. K., et al. 2010, AJ, 140, 1868

Xie, X., Shao, Z., Shen, S., Liu, H., & Li, L. 2016, ApJ, 824, 38

Yu, Q. & Tremaine, S. 2002, MNRAS, 335, 965

Zamanov, R. K., Boeva, S., Nikolov, Y. M., et al. 2017, Astronomische Nachrichten, 338, 680

Zheng, Y., Peek, J. E. G., Putman, M. E., & Werk, J. K. 2019, ApJ, 871, 35